# Plasma Induced Catalytic Conversion of Nitrogen and

# Hydrogen to Ammonia over Zeolitic Imidazolate

# Frameworks ZIF-8, and ZIF-67

- 5 Fnu Gorky, a, Jolie M. Lucero, James M. Crawford, Beth Blake Moises A. Carreon, and Maria L. Carreon\*a
- 8 Joseph St, Rapid City, South Dakota-57701, USA
- 9 b Chemical and Biological Engineering Department, Colorado School of Mines, Golden, CO 8040, USA
- 10 \*Corresponding author: <u>Maria.CarreonGarciduenas@sdsmt.edu</u>
- 12 Keywords: Non-Thermal Plasma, Plasma Catalysis, Ammonia Synthesis, Zeolitic Imidazolate Frameworks,
- 13 Ammonia Adsorption Effect.

4

6

11

- 15 **Abstract**: Microporous crystals have emerged as highly appealing catalytic materials for the assisted plasma
- synthesis of ammonia. Herein, we demonstrate that zeolitic imidazolate frameworks (ZIFs) can act as effective
- catalysts for the synthesis of ammonia via non thermal plasma using an atmospheric dielectric barrier discharge
- 18 (DBD) reactor. We studied two prototypical ZIFs denoted as ZIF-8, and ZIF-67, with uniform crystallographic
- 19 limiting pore apertures of 3.4 Å. The resultant ZIFs displayed ammonia synthesis rates as high as 42.16
- 20 micromoles NH<sub>3</sub>/ min gcat. ZIF-8 displayed remarkable stability upon recycling. The dipole-dipole interactions
- between the polar ammonia molecule and the polar walls of the studied ZIFs led to relatively low ammonia
- 22 uptakes and storage capacity, and to the high observed ammonia synthesis rates. Both ZIFs outperform in
- 23 ammonia synthesis rates other microporous crystals including zeolites, and conventional oxides. Furthermore,

we demonstrate that the addition of Argon to the reactor chamber can be an effective strategy to improve the plasma environment. Specifically, the presence of Argon helped to improve the plasma uniformity making the reaction system more energy efficient by operating at low Specific Energy Input (SEI) range allowing an abundant formation of nitrogen vibrational species.

5

6

7

8

9

10

11

12

13

14

15

16

17

18

19

20

21

22

23

24

25

1

2

3

4

### Introduction

Ammonia is essential for food security due to its use in fertilizers. Ammonia synthesis is currently done using the Haber-Bosch (HB) process typically at ~500 °C and 500 bar, which is the most energy-consuming process in the chemical industry. Global ammonia production (~249.4 million tons) consumes ~1-2% of the world's energy, 2-3% of the world's natural gas output, and emits over 300 million metric tons of CO<sub>2</sub>.<sup>1, 2</sup> With such energy and reaction condition requirements, the HB process is only economically viable at large-scale plants that demand huge capital investments and access to continuous electric power to keep the process continuously running.<sup>3, 4</sup> Consequently, ammonia synthesis is currently centralized, hampering the access of farms in remote areas to affordable fertilizers. The development of simplified alternatives to HB at milder conditions and compatible with intermittent electric power (e.g. from renewable energy sources) is a critical step toward small-scale, decentralized ammonia production. Explored alternatives include decoupling dissociation of H<sub>2</sub> and N<sub>2</sub> in membrane reactors<sup>6</sup> or by proton-based activation of N<sub>2</sub> in electrochemical cells.<sup>7</sup> Electrochemical ammonia synthesis <sup>8</sup> has been driven by the prospect of inexpensive renewable electricity—that would also reduce the carbon footprint of the process—as prices continue to fall (e.g. commercial solar power fell from \$5.36/watt in 2010 to ~\$1.85/watt in 2017). The main issue with electrochemical N<sub>2</sub> reduction is the poor selectivity as H<sub>2</sub> is overwhelmingly the preferred product, with current efforts focused on addressing this issue. 10 The cost-effective implementation of solar and wind sources during the past decade serve as a motivation to look for sustainable alternatives. The implementation of this technology to fully replace fossil fuels for electricity, heat and transportation will be only feasible until there is an effective energy storage and distribution technology. Non-thermal plasma catalysis is an

alternative and transformative process that leverages renewable electricity to produce selectively ammonia at

unprecedented yields. These efforts can lead to the future prospect of the electrification of the chemical industry. 11

4 Currently, the rational engineering of a catalyst for cold plasma environments is emerging as a highly promising

strategy to lead to a sustainable route to produce ammonia<sup>12</sup>. Specifically, the presence of high energy electrons

in plasmas can excite ground state gas molecules that can react efficiently on the surface of selected materials at

lower temperatures and pressures as compared to thermal catalysis. 13 The presence of a suitable active catalyst

for plasma environments can enhance the ammonia production and selectivity.<sup>14-22</sup> Despite all these possible

benefits of plasma catalysis, our current knowledge of proper catalysts for such purposes is very limited.

Furthermore, there is a need to have a better understanding on how different materials behave when exposed to

plasma due to the arise of plasma awaken properties or interactions. In this contribution, we explore the synergy

between ammonia production and ammonia adsorption (storage) in two zeolitic imidazolate frameworks.

The use of crystalline porous phases displaying unimodal micropores are highly appealing for plasma ammonia

synthesis. Recently, our group illustrated the use of microporous crystalline materials, including metal organic

frameworks<sup>23</sup>,and zeolites<sup>24, 25</sup> as catalysts for the synthesis of ammonia via plasma. In these reports, we found

that pore size plays a critical role in the observed catalytic performance. Prompted by this pore size effect, herein

we demonstrate that microporous crystalline phases with smaller crystallographic limiting pore apertures

catalytically outperform microporous crystals having larger pore sizes, and traditional porous oxides. Specifically,

we focus on two representative microporous molecular sieve crystals<sup>26</sup>: ZIF-8, and ZIF-67, with a

crystallographic pore aperture of ~3.4 Å.

# **Experimental Methods**

2

3

5

6

7

8

9

10

11

12

13

14

15

16

17

18

19

20

21

22

23

24

25

# Synthesis of zeolitic imidazolate frameworks

### 1 Synthesis of ZIF-8

- 2 ZIF-8 crystals were synthesized as reported elsewhere.<sup>27</sup> First, the metal solution was prepared by dissolving 0.2
- 3 g of zinc chloride (Acros, 97%), and 0.3 g of sodium formate (Sigma Aldrich, >99%) in 10 g of methanol (Fisher
- 4 Scientific, 99.9%). The organic solution was prepared by dissolving 0.96 g of 2-methylimidazole (Sigma-Aldrich,
- 5 99%) in 10 g of methanol. The two solutions were then mixed together vigorously for 30 minutes at room
- 6 temperature and then added to a Teflon lined stainless steel autoclave and solvothermally treated for 4 hours at
- 7 120°C. The autoclave was then cooled naturally, and the ZIF-8 powder was recovered by centrifugation and
- 8 washed 3x with clean methanol. The powder was then dried at 100°C.
- 9 Synthesis of ZIF-67

12

15

16

- 10 ZIF-67 crystals were synthesized by a slightly different approach as reported elsewhere<sup>28</sup> 5 g of 2-
- methylimidazole (Sigma Aldrich, 99%) was dissolved in 20 mL of DI water. In a second solution, 0.23 g of cobalt
  - (II) nitrate hexahydrate (Sigma Aldrich, 98%) was dissolved in 3 mL of DI water. The two solutions were then
- mixed together vigorously for 15 hours at room temperature. ZIF-67 was then recovered through centrifugation,
- and washed 4x with clean DI water and dried in an oven at 100°C.

### Characterization Methods

- 17 Powder X-Ray diffraction patterns were collected on a Siemens Krystalloflex 810, operated at 25 mA, and 30 kV.
- 18 Scanning Electron Microscopy images were collected on a JEOL-7000 JSM Field Emission microscope operated
- 19 at accelerating voltages of 8-15 kV. ZIFs samples were gold sputter coated to prevent charging. Ammonia
- 20 isotherms were collected on an ASAP 2020 apparatus (Micromeritics) equipped with corrosion resistant Kalrez®
- O-rings (DuPont<sup>TM</sup>). Prior to analysis, ZIF-8 and ZIF-67 were degassed under vacuum at 200 °C. A vacuum
- insulated Dewar with an ice bath at 273 K with equilibration times of at least 10 minutes was used for all samples.
- Nitrogen isotherms were conducted on an ASAP 2020 Plus (Micromeritics) using a liquid nitrogen bath (77 K).
- 24 All samples were degassed for 8 h at 200 °C under high vacuum conditions. Once degassed, the final sample

weight was recorded. All samples were again degassed under high vacuum for 2 h on the analysis port prior to data acquisition. Surface areas were calculated using the Brunauer-Emmett-Teller method.

## **Reactor Setup**

1

2

3 4

5

6

7

8

9

10

11

12

13

14

15

16

17

18

19

20

21

22

23

24

25

26

The catalytic activity of the studied ZIFs was evaluated in a custom designed Dielectric Barrier Discharge (DBD) setup employed in our previous reports.<sup>24, 25, 29</sup> The setup comprises of four parts – the reactor core, emission spectrum capture setup, electrical characterization setup, and a Gas Chromatograph. The complete setup is shown in Figure 1. The reactor core comprises the reactor chamber only. To perform the catalytic tests, nitrogen and hydrogen gases were connected to the reactor using mass flow controllers. The reactor exit gases were sent directly to the GC. The quantification was performed using an Agilent 7820A GC equipped with a HP-PLOTU column (30 m x 0.32 mm x 10 µm) and hydrogen gas as carrier. The gases were bubbled in deionized water to ensure all ammonia is captured and to perform titration as an alternate method of quantification. The high voltage power supply was connected to the reactor using Litz wire and alligator clips. The inner electrode made of tungsten rod (2.4 mm diameter) was placed at the center of the quartz tube with an I.D. of 4 mm and O.D. of 6.40 mm. The fittings were made of PFA (PerFluoroAlkoxy) to avoid any arc formation. The outer electrode made of tinned copper mesh acted as the ground electrode. The length of the plasma zone was  $\sim 8$  cm. The impedance of the chamber was matched to deliver maximum power. The gases flow through the annulus and two quartz frits were placed carefully such that they do not cause any pressure increase. 100 mg of catalyst were loaded as a fine powder in the reactor. The reactor was purged with a nitrogen and hydrogen mixture to remove oxygen after the reactor was sealed. The plasma-catalyst intersection zone was approximately 6 cm long. The catalyst was packed in the overlap area between the inner and outer electrodes. The reactions were carried out at different feed flow rates ranging from 3:1 to 1:6 ratio of nitrogen to hydrogen (N<sub>2</sub>:H<sub>2</sub>) with a total flow rate of 25 sccm at various applied voltages ranging from 7 to 21 kV<sub>pk-pk</sub>. We kept the average bulk temperature of the reactor at the average value of 98 °C (± 1.2 °C) with the use of a fan continuously running during the reaction time. The ammonia yield refers to the degree of nitrogen fixation (conversion) as compared to the nitrogen content in the feed. This yield

is calculated by taking the ratio of the ammonia synthesis rate to the nitrogen flow rate in the feed on a molar basis. To determine the ammonia synthesis rate, the exhaust gas was sent to the gas chromatograph calibrated for ammonia synthesis. The calibration curve details are provided in **Table S1 and Figure S1**. The reactor was connected to an oscilloscope to obtain the current and voltage waveforms. A Tektronix 2048 series oscilloscope was used along with a Tektronix P6015A high voltage probe having a 1000X voltage reducing rating. The current was measured by a 10X current reducing probe to get the waveforms. The energy delivered to the reactor was calculated based on these measurements.

The light emitted from the discharge was led through an optical system and the emission spectra of the glow region were measured at the center of the tube. The measurements were recorded using a dual channel UV-VIS-NIR spectrophotometer in scope mode (Avantes Inc., USB2000 Series). The spectral range was from 200-1100 nm, using a line grating of 600 lines/mm and resolution of 0.4 nm. A bifurcated fiber optic cable with 400 μm was employed.

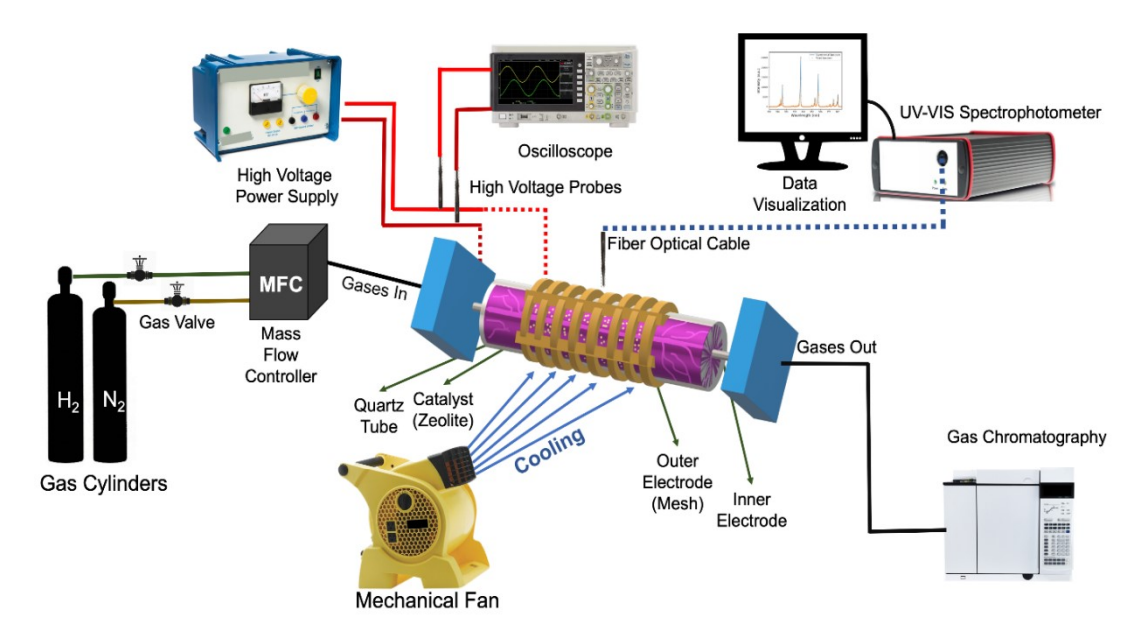
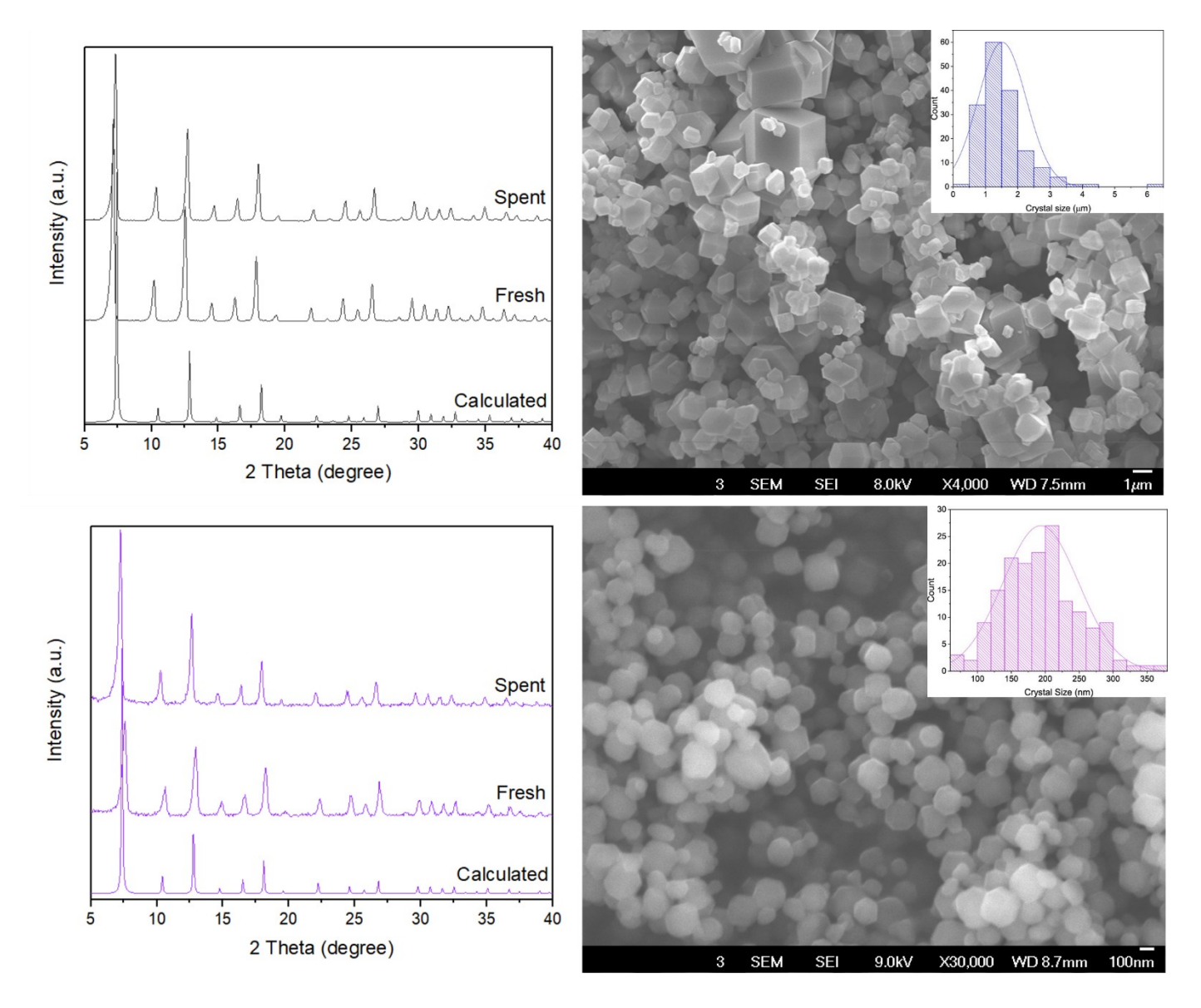


Figure 1. Schematic of the Dielectric Barrier Discharge (DBD) reactor setup employed in this study

Figure 2 shows the XRD patterns and representative SEM images of the ZIF crystals. Figure 2a shows the XRD pattern of ZIF-8 displaying the known sodalite phase of this zeolitic imidazolate framework. Figure 2b shows ZIF-8 crystals with a broad size distribution in the 1-10 μm range. Figure 2c illustrates the XRD pattern of ZIF-

67, which is in well agreement with sodalite topology. These ZIF-67 crystals display sizes within the 0.1- $0.3 \mu m$  range as shown in **Figure 2d.** 



**Figure 2.** XRD patterns of (a) ZIF-8 and (c) ZIF-67 and representative SEM images of (b) ZIF-8 and (d) ZIF-67 microporous crystals employed as catalysts in this study. **Insets correspond to histograms showing crystal size distribution**.

The experimental BET surface areas for ZIF-8 and ZIF-67 were 1880 m<sup>2</sup>/g and 1674 m<sup>2</sup>/g respectively. The observed surface areas are within the typical ranges reported in the literature for these microporous crystals.

1 The chosen porous crystals illustrate an example of a representative microporous crystalline molecular sieve

hybrid frameworks with similar crystallographic pore apertures. ZIF-8 is a metal organic framework formed by

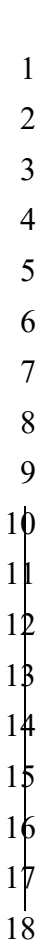
linking zinc ions with nitrogen atoms of imidazole-based groups resulting in a microporous crystalline structure

displaying sodalite topology<sup>30</sup> ZIF-67 is isostructural to ZIF-8, with the difference that Zn ions are replaced by

Cobalt ions.<sup>30</sup> The crystallographic limiting pore aperture of both ZIFs is 3.4 Å.

## Plasma Catalytic Activity over ZIF-8 and ZIF-67

The experiments were first carried out without any catalyst (plasma only). The reactions were repeated three times and run at ~94 °C (average temperature maintained with the use of a fan) and atmospheric pressure. To understand the catalytic effect of the microporous materials and differentiate it from the only plasma effect, all the catalysts were tested at similar flow rate  $N_2$ : $H_2$  (1:3) as shown in **Figure 3**. ZIF-67 and ZIF-8 displayed ammonia synthesis rates of 26.65 micromoles of NH<sub>3</sub>/min gcat and 28.52 micromoles of NH<sub>3</sub>/min gcat respectively. In this Figure, we compare the catalytic performance (at the same reaction conditions) vs other catalysts reported by our group such as zeolite beta<sup>25</sup>, zeolite  $5A^{25}$ , alumina<sup>25,29</sup> and silica<sup>25,29</sup> It is evident that both ZIFs display higher ammonia synthesis rates. When comparing with plasma only (0.386 micromol/min) the synthesis rate is ~ 70 times higher with a ZIF in the reaction chamber. The active sites of the ZIFs are the -C=-C- of the imidazole group of the linker, which is known to be the only polarizable group. The higher ammonia polarizability as compared to nitrogen and hydrogen leads to van der Waals interactions with this -C=-C- group. In principle, metal sites in the ZIFs may not be accessible for the gas molecules due to the steric hindrance by the surrounding ligands.



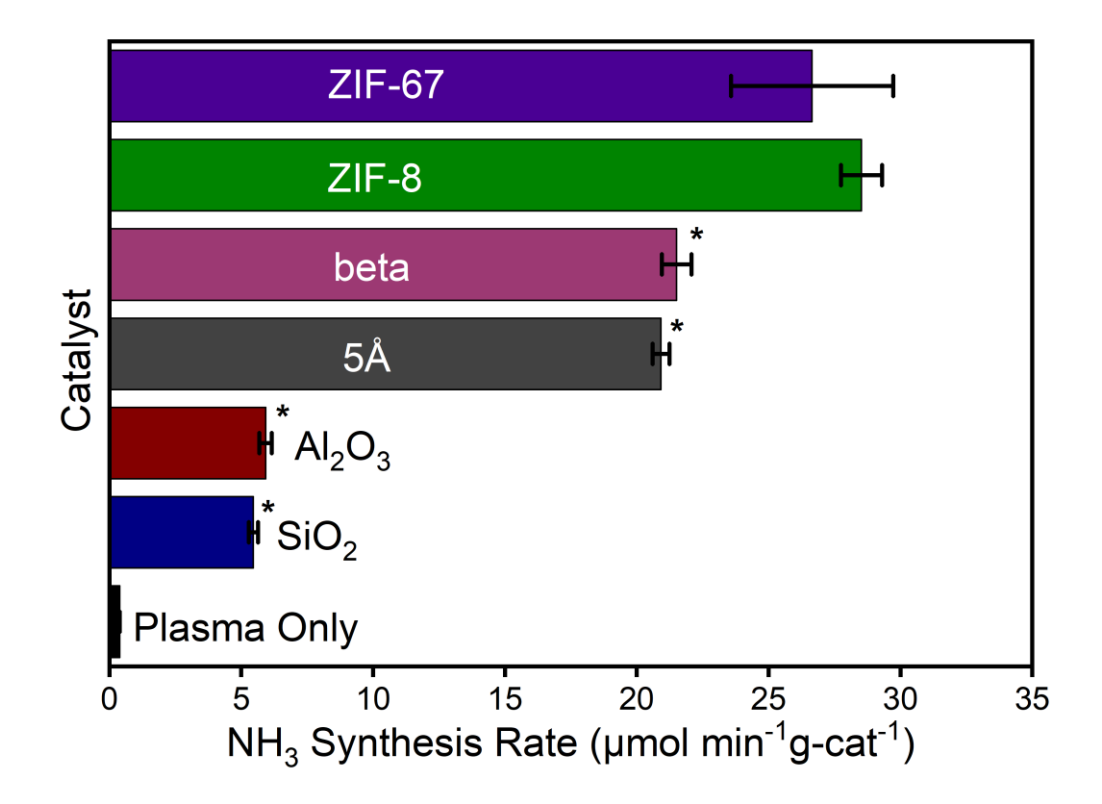


**Figure 3.** Ammonia synthesis rate performance for the studied ZIF crystals at 1:3 ( $N_2$ : $H_2$ ) feed ratio. For comparison other \*zeolites (beta, and 5A)<sup>25</sup>, and \*oxides ( $Al_2O_3$ ,  $SiO_2$ )<sup>25, 29</sup> & plasma only have been included.

### Ammonia Adsorption on ZIF-8 and ZIF-67.

To better understand the influence of adsorption properties on the catalytic behavior of the ZIF catalysts, ammonia isotherms were collected at 273 K (**Figure 4**). Both ZIFs display similar low ammonia uptakes. The *weaker dipole-dipole interactions* between the polar ammonia molecule and the polar walls of both ZIFs due to the presence of uncoordinated nitrogen of the organic linker (2 methyl imidazole) may be responsible for the lower observed ammonia uptakes. The low ammonia uptakes correlate with the high observed ammonia synthesis rates. In other words, low concentration of ammonia is stored (uptake) with the ZIF frameworks, leading to high ammonia synthesis rates. In the case of ZIF-8, and ZIF-67, the presence of an active metal (Zn and Co respectively) may help to promote higher ammonia synthesis rates. It is known that some transition metals are active species for ammonia synthesis via thermal catalysis.<sup>31-33</sup> Furthermore, Co has been identified as an effective metal for plasma catalytic ammonia synthesis.<sup>14, 15</sup>

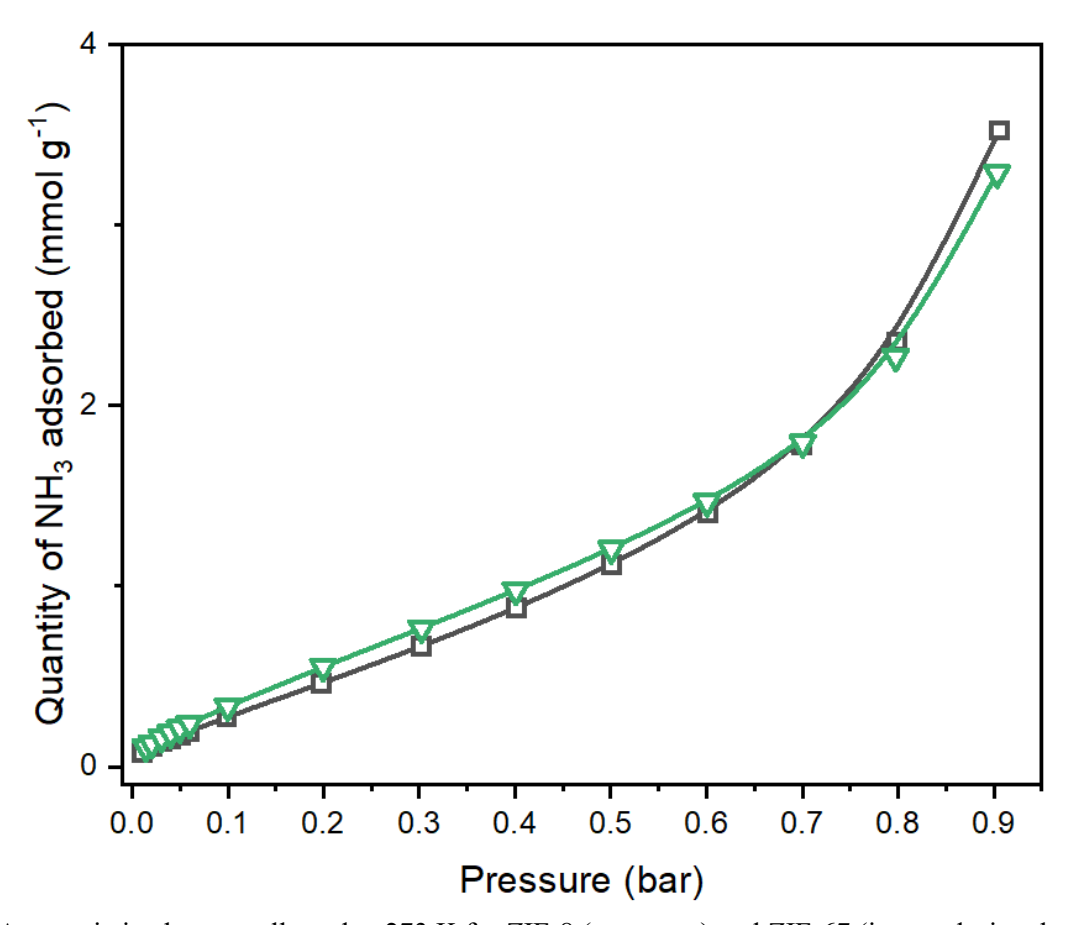


**Figure 4.** Ammonia isotherms collected at 273 K for ZIF-8 (square,  $\Box$ ) and ZIF-67 (inverted triangle,  $\nabla$ ).

## **ZIF8 and ZIF-67 Stability**

Both ZIF catalysts were recovered and recycled after reaction. The recycling process consisted in thermal treatment at 200°C after plasma exposure in a furnace for  $\sim$  2 hours. The recycled catalysts (spent) were catalytically evaluated. **Figure 5** compares the catalytic performance of the fresh vs the spent catalysts at 15 minutes for a total flow rate of 25 sccm with 1:3 (N<sub>2</sub>:H<sub>2</sub>) feed ratio. ZIF-8 displayed remarkable catalytic stability after recycling. In the case of ZIF-67, a reduction of catalytic activity was observed.

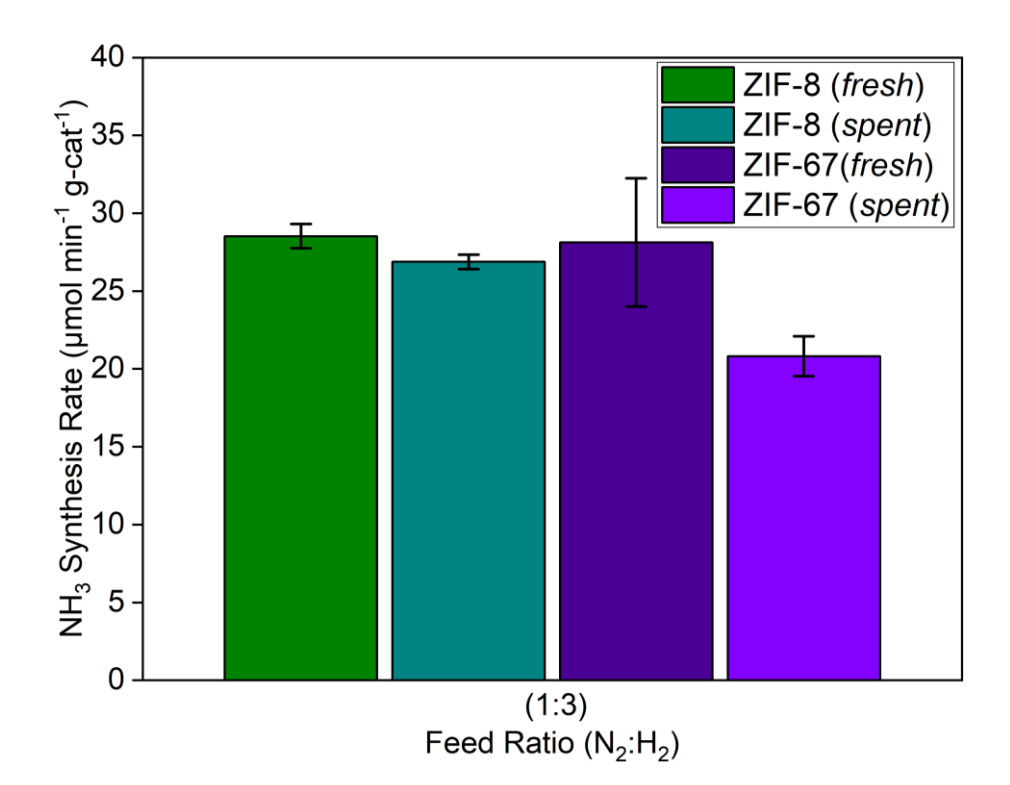
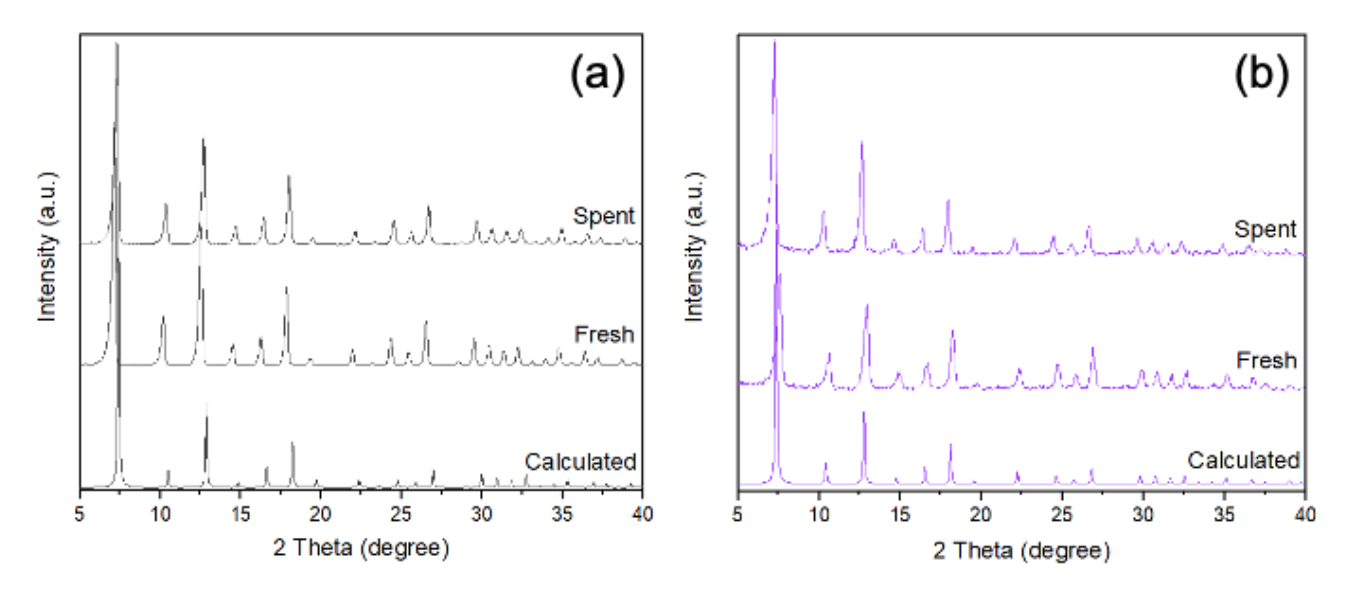


Figure 5. Ammonia Synthesis rate for fresh vs. spent ZIF catalysts at 15 minutes and 1:3 (N2:H2) feed ratio.

XRD patterns of the spent catalysts are shown in **Figure 6**. For both spent ZIFs, the XRD patterns remained similar to their respective fresh catalysts. In other words, the structural stability of both ZIFs was preserved after plasma treatment. Furthermore, the morphology of the spent crystals remained the same (**Figure S4**), confirming the stability of both ZIFs.

Zeolitic imidazolate frameworks are one of the most chemically stable metal organic frameworks. Its enhanced chemical stability is associated to their metal-ligand bond strength. It is known that stable metal organic frameworks are formed by coordinating soft divalent metals such as Zn<sup>2+</sup>, and Co<sup>2+</sup> with imidazolates.<sup>34</sup> In the case of the spent ZIF-67 sample, a slight shift of the XRD peaks to lower 2 theta angles suggests unit cell expansion. This unit cell expansion for ZIF-67 spent sample led to higher ammonia uptakes as shown in **Figure 7**, and therefore to lower ammonia synthesis rates.

In the case of the spent ZIF-8 sample, the ammonia uptake remained constant, which agrees well with the minimum catalytic decay of the ZIF-8 spent sample. **Figure 7** shows the ammonia isotherms for fresh and spent ZIFs. Details on kinetics data for the spent materials are summarized in **Figures S2-84**.



**Figure 6.** XRD pattern for a) ZIF-8, b) ZIF-67 samples fresh, spent and simulated pattern tested at 1:3 (N<sub>2</sub>:H<sub>2</sub>) ratio.

The nitrogen adsorption desorption isotherms for the fresh and spent ZIF catalysts is shown in Figure S5.

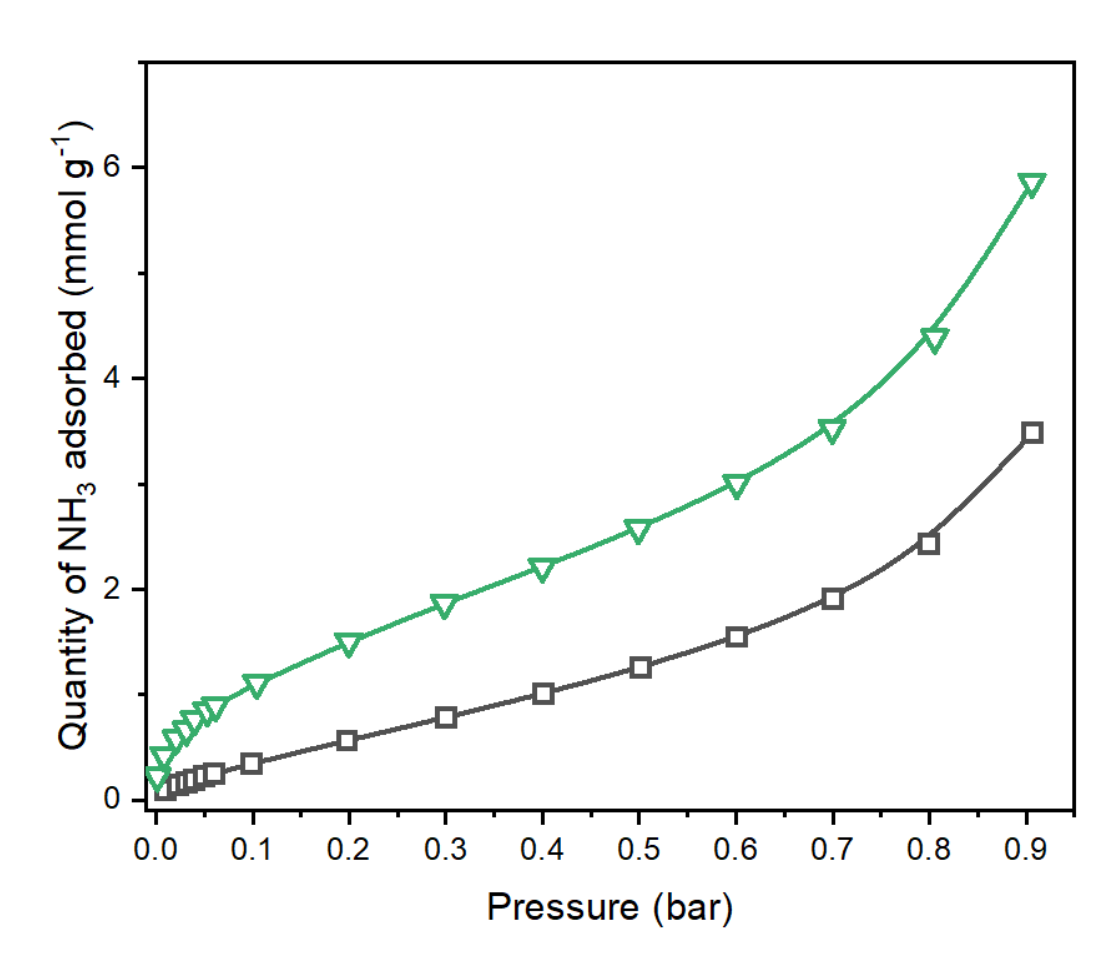


**Figure 7.** Ammonia isotherms collected at 273 K for spent ZIF-8 (square,  $\Box$ ) and spent ZIF-67 (inverted triangle,  $\nabla$ ).

# **Optimizing the Plasma Environment**

One of the main challenges when dealing with a DBD atmospheric reactor is the *non-uniformity of the plasma*. In fact, the optimization of the plasma environment is one of the grand challenges to overcome in order to improve the plasma mediated ammonia synthesis. The use of noble gases such as Argon (Ar), is a strategy that has been employed to improve plasma homogeneity.<sup>19, 35</sup> Therefore, we introduced Ar to the chamber at a ratio of 1N<sub>2</sub>: 1.5H<sub>2</sub>: 1.5Ar. The presence of Ar can increase the plasma discharge intensity and uniformity<sup>19</sup>. This might be attributed to the charge transfer reaction between Ar+ with N<sub>2</sub>. In addition, the plasma homogeneity induced by Ar can result in a higher probability of having electrons with the energy necessary to readily activate the N<sub>2</sub>

molecule. Therefore, a reduction in the required energy might be achieved as the power directed for reactant activation might be employed more efficiently. Interestingly, as shown in **Figure 8**, we observed an increase in the ammonia synthesis rate when employing Ar. For instance, at 15 minutes the ammonia synthesis rates in the presence of Ar increased from 28.52 to 34.27 micromoles of NH<sub>3</sub>/min gcat for ZIF-8 and from 28.12 to 41.68 micromoles of NH<sub>3</sub>/min gcat for ZIF-67. Furthermore, the presence of Ar stabilized the ammonia synthesis rate as a function of time.

8 T

The benefit of employing noble gases together with small particle size catalysts has been demonstrated in other plasma catalytic synthesis involving CO<sub>2</sub> reduction in packed beds<sup>36</sup>. This report demonstrated that the addition of Ar to CO<sub>2</sub> reduces the burning voltage of the mixtures allowing discharges to form in packed void spaces at lower voltages that would typically occur in pure CO<sub>2</sub>. <sup>24</sup> In our case, a similar beneficial effect in the discharge may be achieved when adding Ar.

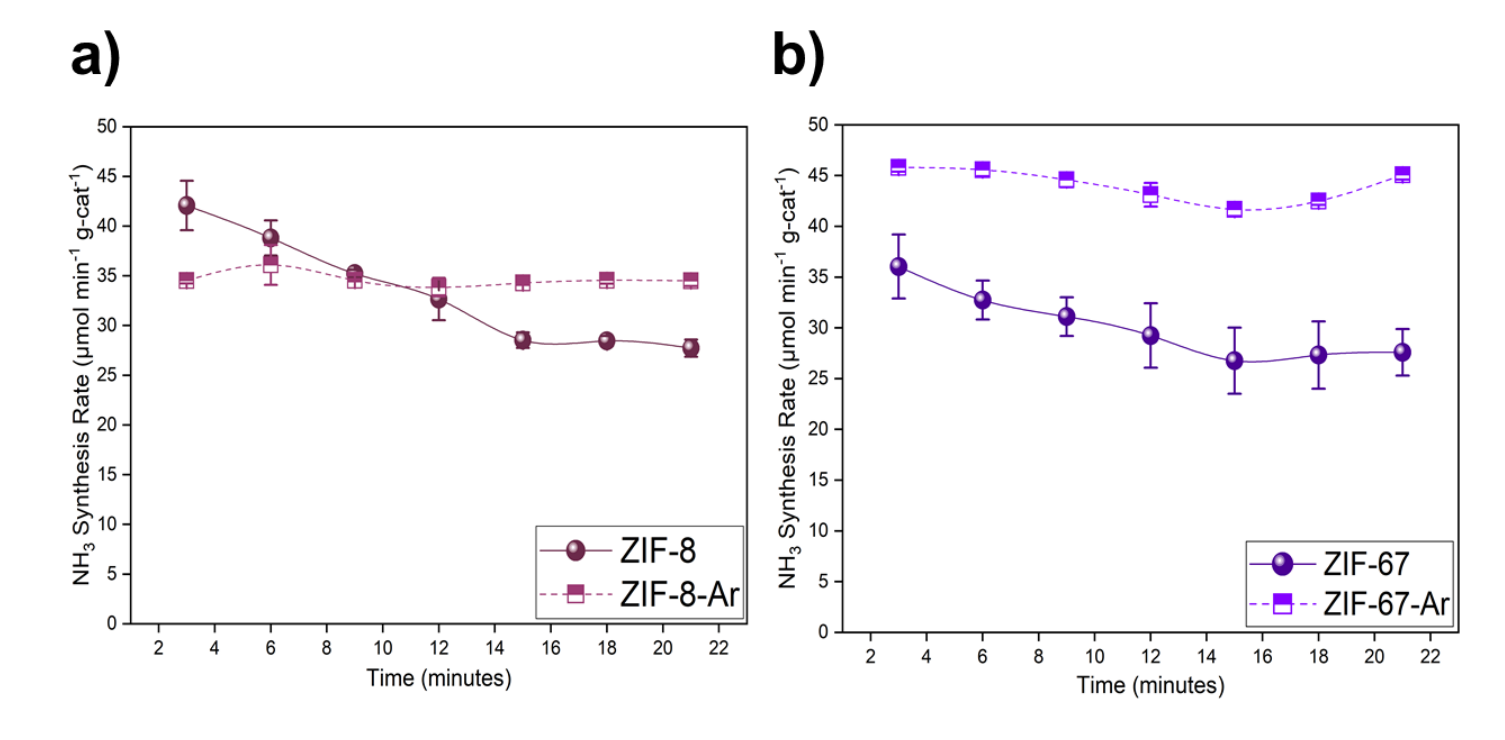


**Figure 8.** Ammonia synthesis rate performance for the studied ZIFs at 1:3 ( $N_2$ : $H_2$ ) feed ratio and 1:1.5:1.5 ( $N_2$ : $H_2$ :Ar).

- 1 Figure 9 compares the ammonia synthesis rate vs specific energy input (kJ/L) for several fresh catalysts
- 2 (including the studied ZIFs) evaluated at the same 1:3 (N<sub>2</sub>:H<sub>2</sub>) ratio when employing the same reaction system.
- 3 The specific energy input (SEI) in kJ/L is defined as the measured power in kW divided by the input flow ratio to
- 4 the reactor in liters per minute (for electrical characterization details of the reactor refer to **Figure S4**):

9

12

- 6 SEI(kJ/L)= Power (kW)/ Flow rate (L/min)\* (60s/1min)
- 7 It is evident from **Figure 9** that in ZIF-8 and ZIF-67, the measured watts are lower when using Ar which results
- 8 in lower SEI numbers. Furthermore, higher ammonia synthesis rates were observed as well, as discussed
  - previously. ZIF-8 and ZIF-67 show the highest ammonia synthesis rates (34.27 micromoles of NH<sub>3</sub>/min gcat and
- 41.68 micromoles of NH<sub>3</sub>/min gcat respectively) while the calculated specific energy input was 37.34 kJ/L and
- 42. 81 kJ/L for each material respectively when employing a mixture with Argon. The SEI values and synthesis
  - rates for these materials without Argon were 60.79 kJ/L and 28.52 micromoles of NH<sub>3</sub>/min gcat for ZIF-8 and
- 13 75.52 kJ/L and 28.12 micromoles of NH<sub>3</sub>/min gcat for ZIF-67. Both ZIFs, showed higher ammonia synthesis rates
- as compared to other materials that do not contain a metal and that where explored by our group previously.<sup>24, 25,</sup>
- 15 <sup>29</sup> However, it should be noted that when employing ZIF-8 and ZIF-67 the ammonia synthesis rates are not very
  - different within the experimental error range. This suggests that the topology, and textural properties (among other
- properties) of the ZIFs, may play are more important role for the plasma catalytic synthesis of ammonia that the
- 18 transition metal itself.

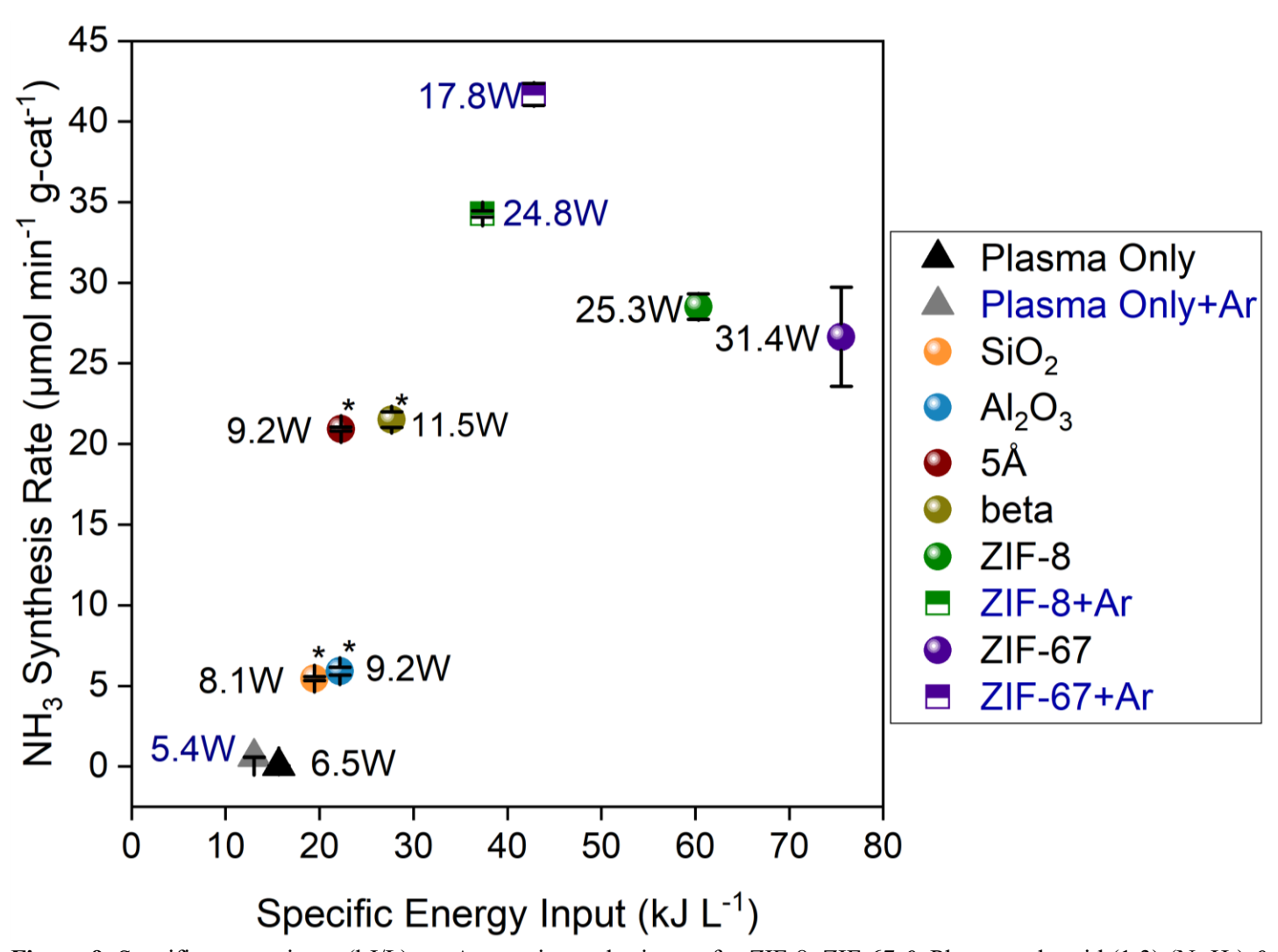


**Figure 9.** Specific energy input (kJ/L) vs. Ammonia synthesis rate for ZIF-8, ZIF-67 & Plasma only with(1:3) (N<sub>2</sub>:H<sub>2</sub>) & without Argon (1:1.5:1.5) (N<sub>2</sub>:H<sub>2</sub>:Ar) (This work), 5A\*, beta\*, Al<sub>2</sub>O<sub>3</sub>\*, SiO<sub>2</sub>\*25, 29 tested at 1:3 (N<sub>2</sub>:H<sub>2</sub>) feed ratio.

## **Emission Spectroscopy Analysis**

To have a better understanding on the role of the gas phase species in the plasma synthesis of ammonia, optical emission spectra of the DBD was collected at the feed ratio 1:3 ( $N_2$ : $H_2$ ) for ZIF-67 with and without Ar (**Figure 10**). We chose ZIF-67 due to its better catalytic performance as compared to the other microporous crystals. It can be observed that the registered peaks when using Ar are about two times more intense than without Ar. The data shown in **Figure 10** was collected at equal applied voltages and same frequency. Interestingly, the identification of N atomic species ( $2p^23p \rightarrow 2p^23s$ ) and  $H\alpha$  Balmer atomic species suggest the dissociation of  $N_2$  and  $H_2$ . This has been previously reported for ammonia synthesis in a DBD reactor<sup>37</sup>. The  $N_2$ <sup>+</sup> plasma excited

- species (337.1nm and 391.4nm) show higher intensity values compared to atomic nitrogen (746.8nm). Moreover,
- 2 we observed that with the addition of Ar, the formation of  $N_2^+$  increased as observed in the UV-Vis spectra. These
- $N_2$  plasma excited species intensity is around 2 times higher with Ar than without Ar. The non-thermal plasma
- 4 approach herein presented is focused on maximizing the density of mildly plasma activated nitrogen species that
- 5 require lower energy input as compared to nitrogen radicals. These results suggest that the presence of Ar favors
- a higher concentration of nitrogen vibrational species that require lower activation energy than atomic nitrogen.
- 7 Typically, mild activation of nitrogen can be achieved at relatively low SEI values, which agrees well with our
- 8 results shown in **Figure 9**.

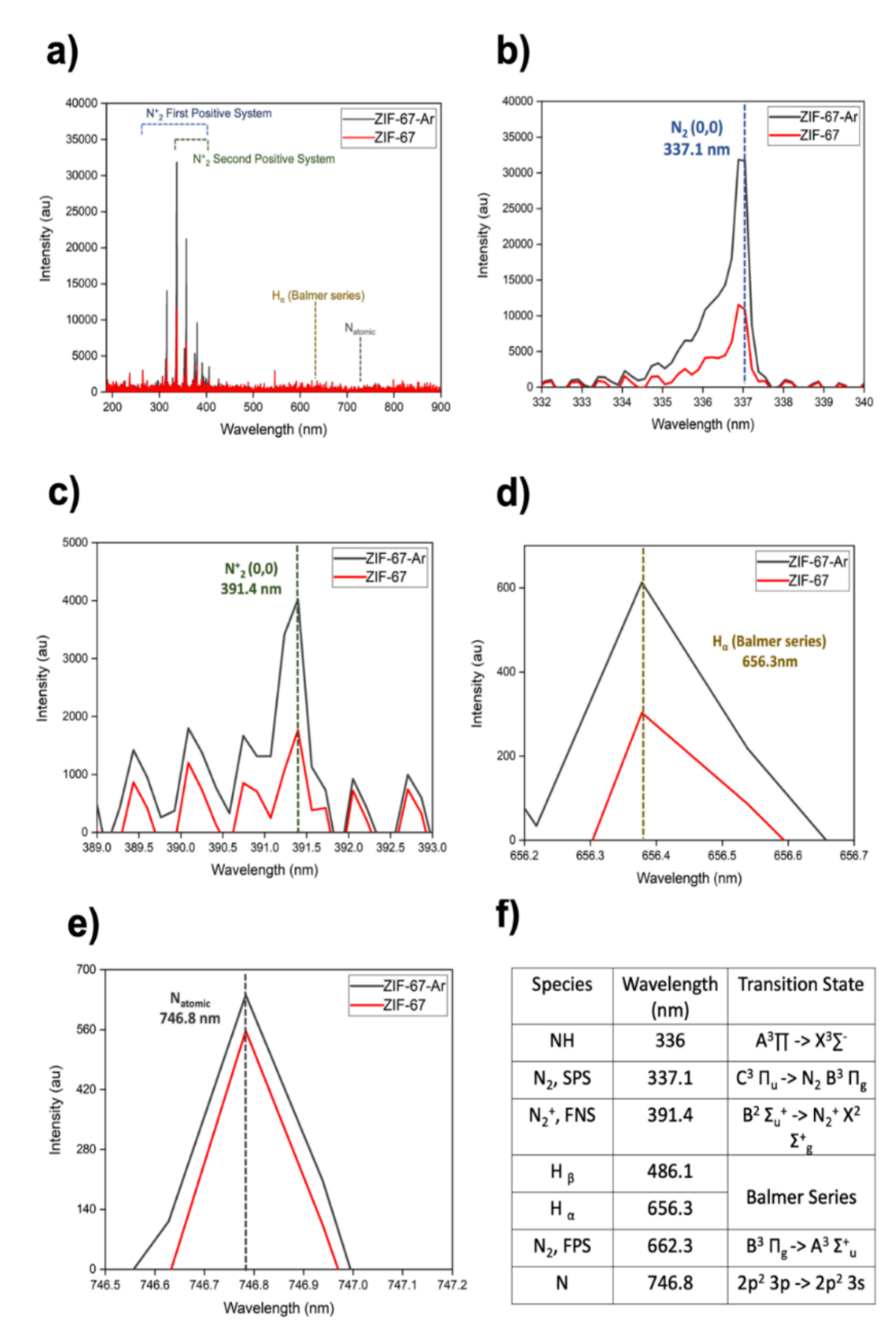


**Figure 10.** ZIF-67 Emission spectra collected during plasma catalytic ammonia synthesis (a) Comparative analysis on ZIF-67 at 1:3  $N_2$ : $H_2$  feed ratio & diluted 1:1.5:1.5  $N_2$ : $H_2$ :Ar feed ratio at constant frequency of 25 kHz, (b) Emission spectra of  $N_2$ , (c) Emission spectra of  $N_2^+$ , (d) Emission spectra of  $H_\alpha$ , (e) Emission spectra of  $H_\alpha$ .

### **Constant energy input experiments**

We carried out selected experiments at two constant watt conditions of 5 (7-8 kV<sub>pk-pk</sub>) and 10 watts (9.8-11 kV<sub>pk-pk</sub>). Note that previous data presented in this manuscript was obtained at 25 kHz constant frequency for 15 Watts (12-15 kV<sub>pk-pk</sub>) to 35 Watts (18-21 kV<sub>pk-pk</sub>). By forcing the input energy (watts) to 5 W and 10 W, respectively, we were able to observe that at constant watts, again ZIF-67 with a mixture of 1:1.5:1.5 N<sub>2</sub>:H<sub>2</sub>:Ar feed ratio performs the best. Hence, it is the most energy efficient (as compared to ZIF-8). Specifically, at 5 watts ZIF-67-Ar produced 20.04 micromoles of NH<sub>3</sub>/min gcat, and at 10 watts ZIF-67-Ar produced 24.91 micromoles of NH<sub>3</sub>/min gcat. Constant energy input experiments are summarized in **Figure 11**.

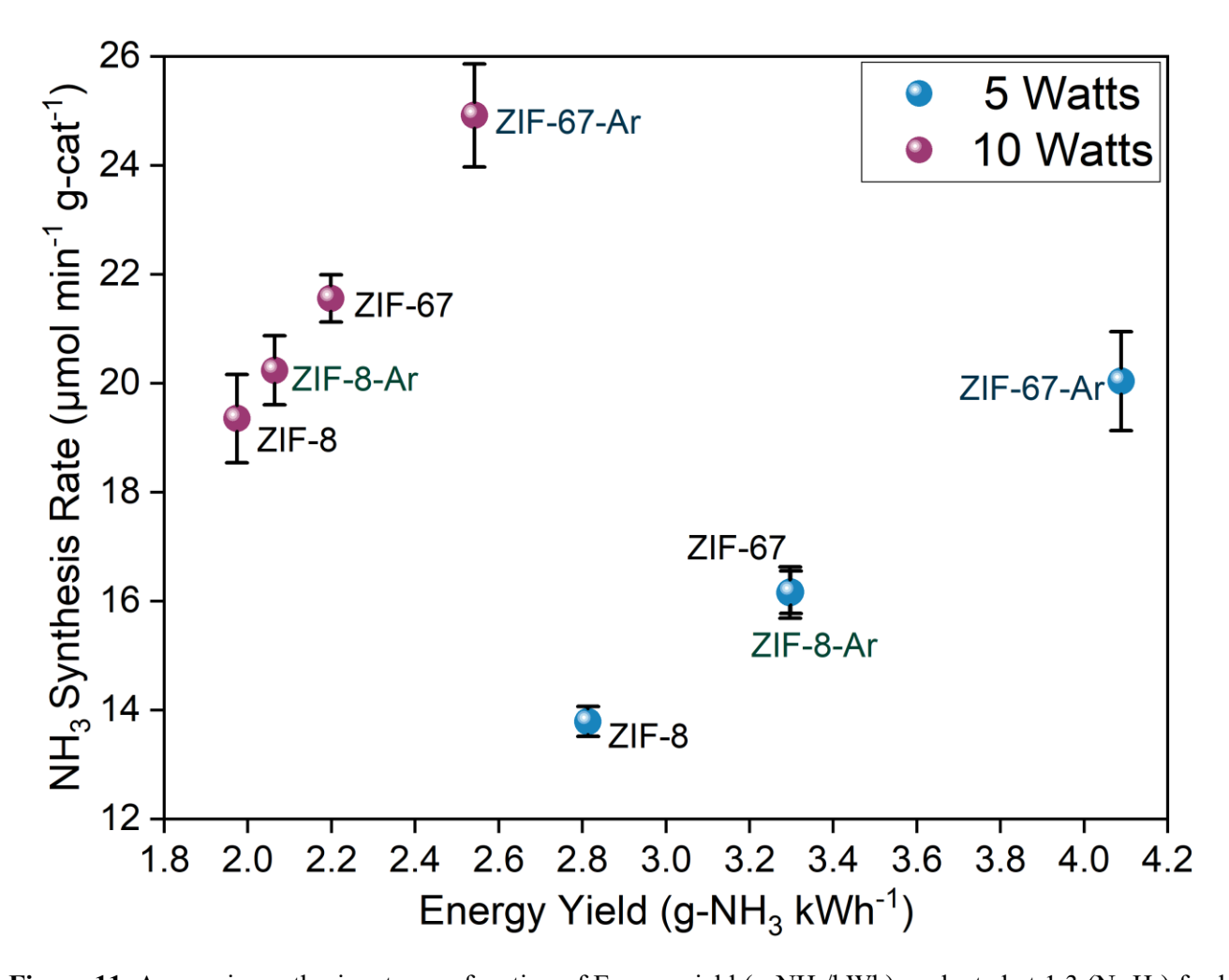


**Figure 11.** Ammonia synthesis rate as a function of Energy yield (g-NH<sub>3</sub>/kWh) evaluated at 1:3 (N<sub>2</sub>:H<sub>2</sub>) feed ratio., and two constant watts conditions: 5 and 10 watts.

To determine the main difference in the gas phase when having the extreme performing points, i.e. only plasma and ZIF-67, we collected the optical emission spectra of the DBD at the feed ratio 1:3 ( $N_2$ : $H_2$ ) for only plasma and ZIF-67 with and without Ar (**Figure 12**). These emission spectra were collected at the constant energy input of 10 W (9.8-11 kV<sub>pk-pk</sub>). Interestingly, the ZIF-67 & only plasma with Ar showed the highest intensity peaks for  $N_2$  (337.1nm) and  $N_2$ <sup>+</sup> (391.4nm) in comparison with the gas phase with no Ar at the same conditions. One should recall that  $N_2$ <sup>+</sup> (391.4nm) is considered one of the most important nitrogen precursors in the plasma catalytic ammonia synthesis. The intensity of  $N_2$ <sup>+</sup> (391.4nm) was observed to be higher when Ar is in the chamber than

when it is absent.

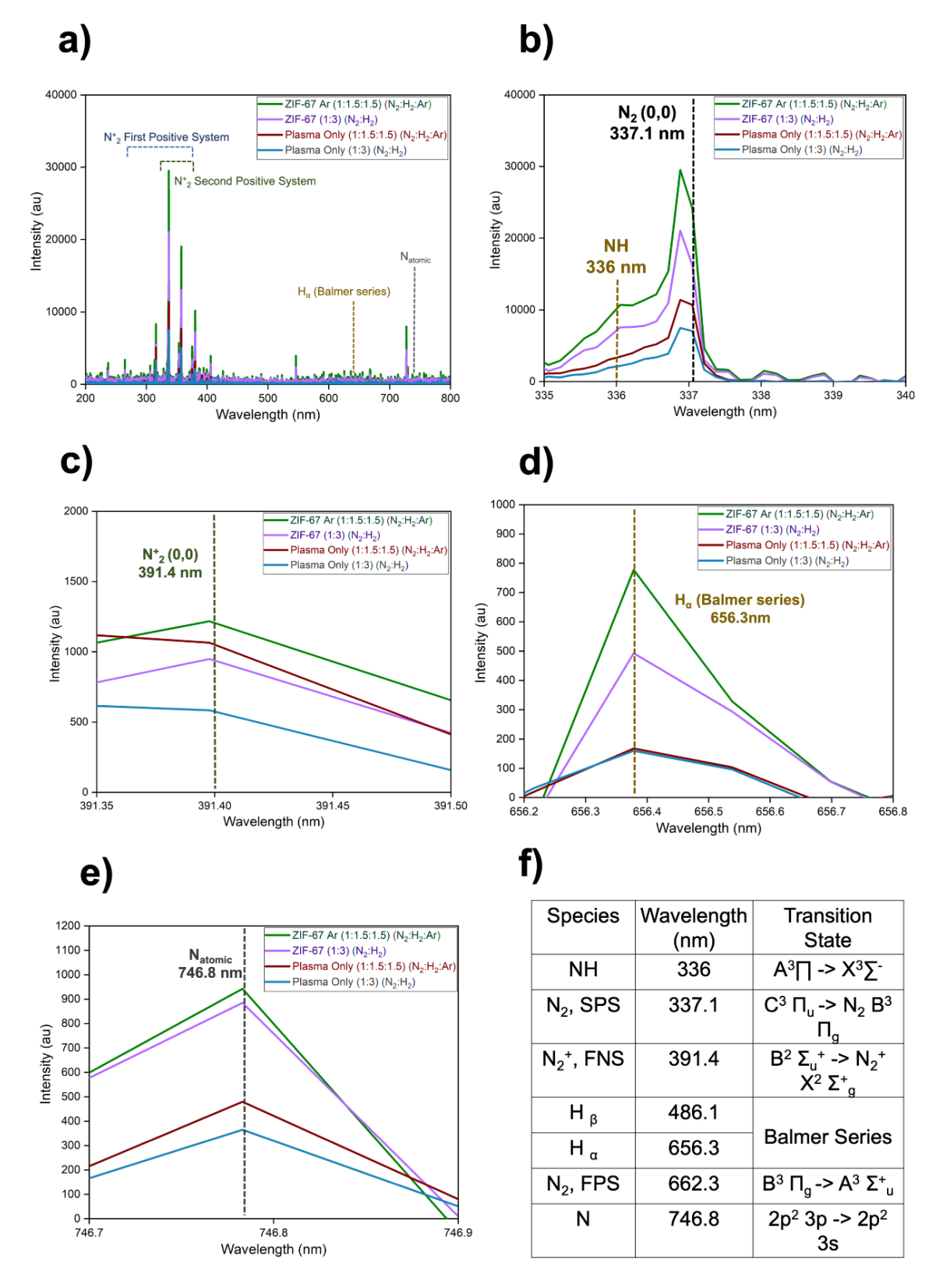


Figure 12. Emission spectra collected during plasma catalytic ammonia synthesis (a) Comparative analysis on Plasma Only and ZIF-67 at 1:3  $N_2$ : $H_2$  feed ratio & diluted 1:1.5:1.5  $N_2$ : $H_2$ :Ar feed ratio at constant watts of 10 W, (b) Emission spectra of  $N_2$ , (c) Emission spectra of  $N_2^+$ , (d) Emission spectra of  $H_\alpha$ , (e) Emission spectra of  $N_{atomic}$  and f) summary of important plasma species.

### Conclusions

In summary, we demonstrate that ZIF-8 and ZIF-67 microporous crystals can act as effective catalysts for the synthesis of ammonia via non thermal plasma using an atmospheric DBD reactor. Specifically, we studied two prototypical zeolitic imidazolate frameworks denoted as ZIF-8, and ZIF-67with crystallographic pore size of 3.4 Å. The studied ZIFs displayed ammonia synthesis rates as high as 42.16 micromoles NH<sub>3</sub>/ min gcat. ZIF-8 displayed remarkable stability upon recycling. The dipole-dipole interactions between the polar ammonia molecule and the polar walls of ZIF-8 and ZIF-67 led to relatively low ammonia storage capacity, and therefore to high observed ammonia synthesis rates. The studied ZIFs, outperform in ammonia synthesis rates other microporous crystals including zeolites , and traditional oxides. To improve plasma uniformity, Argon was introduced in the reaction chamber. The presence of Argon resulted in synthesis rates ~1.2 times higher than without argon for both ZIFs. Moreover, the calculated Specific Energy Input (SEI) values were ~1.6 times smaller with Argon. This lower observed SEI values translated in a higher concentration of plasma vibrational activated nitrogen species that require lower energy than atomic nitrogen. Therefore, Argon helped to improve the energy efficiency of the reactor system by allowing its operation in a low SEI range allowing the formation of less energetic consuming nitrogen vibrational species.

- 1 ASSOCIATED CONTENT
- 2 Supporting Information.
- 3 Details on Ammonia Calibration Curve, Performance of Spent materials SEI Vs. Synthesis rate, Performance of
- 4 spent materials with and without Argon, Details on Reactor Electrical Characterization with Lissajous curve for
- 5 Plasma only, ZIF-8, ZIF-67.

7 Corresponding Author

6

8

- \*Corresponding author: Maria.CarreonGarciduenas@sdsmt.edu
- 10 ACKNOWLEDGMENT
- Maria L. Carreon thanks NSF-CBET award No. 1947303. M.A. Carreon acknowledges Department of Energy
- Office of Science DE-SC0021357. We thank Prof. Manika Prasad and graduate student Gama Firdaus from the
- 13 Colorado School of Mines Geophysics Department for their support with adsorption measurements.

### References

1

2

7

8

11

12

13

14

15

16

17 18

19

20

21

22

23

24

27

32

33

34

35

43

- 1. Tanabe, Y.; Nishibayashi, Y., Developing more sustainable processes for ammonia synthesis. 4. Coordination Chemistry Reviews **2013**, 257 (17), 2551-2564.
- 5 2. <a href="http://ictpost.com/global-ammonia-capacity-to-reach-250-million-tons-per-year-by-2018/">http://ictpost.com/global-ammonia-capacity-to-reach-250-million-tons-per-year-by-2018/</a>, Global Ammonia capacity to reach 250 million tons per year by 2018. 2015.
  - 3. Erisman, J. W.; Sutton, M. A.; Galloway, J.; Klimont, Z.; Winiwarter, W., How a century of ammonia synthesis changed the world. *Nature Geoscience* **2008**, *1* (10), 636.
- 9 4. Schlogl, R., Ammonia Synthesis in:" Handbook of Heterogeneous Catalysis. *Department of Inorganic Chemistry, Fritz-Haber-Institute of the MPG, Germany* **1991**.
  - 5. Patil, B., Plasma (catalyst)-assisted nitrogen fixation: reactor development for nitric oxide and ammonia production. **2017**.
  - 6. Mizushima, T.; Matsumoto, K.; Ohkita, H.; Kakuta, N., Catalytic effects of metal-loaded membrane-like alumina tubes on ammonia synthesis in atmospheric pressure plasma by dielectric barrier discharge. *Plasma Chemistry and Plasma Processing* **2007**, *27* (1), 1-11.
  - 7. Skodra, A.; Stoukides, M., Electrocatalytic synthesis of ammonia from steam and nitrogen at atmospheric pressure. *Solid State Ionics* **2009**, *180* (23), 1332-1336.
  - 8. Mukherjee, S.; Cullen, D. A.; Karakalos, S.; Liu, K.; Zhang, H.; Zhao, S.; Xu, H.; More, K. L.; Wang,
  - G.; Wu, G., Metal-organic framework-derived nitrogen-doped highly disordered carbon for electrochemical ammonia synthesis using N2 and H2O in alkaline electrolytes. *Nano Energy* **2018**, *48*, 217-226.
  - 9. Fu, R.; Feldman, D. J.; Margolis, R. M.; Woodhouse, M. A.; Ardani, K. B. *US solar photovoltaic system cost benchmark: Q1 2017*; National Renewable Energy Lab.(NREL), Golden, CO (United States): 2017.
  - 10. Hu, L.; Khaniya, A.; Wang, J.; Chen, G.; Kaden, W. E.; Feng, X., Ambient electrochemical ammonia synthesis with high selectivity on Fe/Fe oxide catalyst. *ACS Catalysis* **2018**, *8* (10), 9312-9319.
- 25 11. Rouwenhorst, K. H. R.; Engelmann, Y.; van't Veer, K.; Postma, R. S.; Bogaerts, A.; Lefferts, L., Plasma-driven catalysis: green ammonia synthesis with intermittent electricity. *Green Chemistry* **2020**, *22* (19),
  - 6258-6287.
- 28 12. Carreon, M. L., Plasma catalytic ammonia synthesis: state of the art and future directions. *Journal of Physics D: Applied Physics* **2019**, *52* (48), 483001.
- Neyts, E. C.; Ostrikov, K.; Sunkara, M. K.; Bogaerts, A., Plasma catalysis: synergistic effects at the nanoscale. *Chemical reviews* **2015**, *115* (24), 13408-13446.
  - 14. Mehta, P.; Barboun, P.; Herrera, F. A.; Kim, J.; Rumbach, P.; Go, D. B.; Hicks, J. C.; Schneider, W.
  - F., Overcoming ammonia synthesis scaling relations with plasma-enabled catalysis. *Nature Catalysis* **2018**, *I* (4), 269-275.
  - 15. Barboun, P.; Mehta, P.; Herrera, F. A.; Go, D. B.; Schneider, W. F.; Hicks, J. C., Distinguishing Plasma
- Contributions to Catalyst Performance in Plasma-Assisted Ammonia Synthesis. *ACS Sustainable Chemistry & Engineering* **2019**, *7* (9), 8621-8630.
- 38 16. van't Veer, K.; Reniers, F.; Bogaerts, A., Zero-dimensional modeling of unpacked and packed bed
- dielectric barrier discharges: the role of vibrational kinetics in ammonia synthesis. *Plasma Sources Science and Technology* **2020**, *29* (4), 045020.
- 41 17. Herrera, F. A.; Brown, G. H.; Barboun, P.; Turan, N.; Mehta, P.; Schneider, W. F.; Hicks, J. C.; Go,
- D. B., The impact of transition metal catalysts on macroscopic dielectric barrier discharge (DBD) characteristics
  - in an ammonia synthesis plasma catalysis reactor. Journal of Physics D: Applied Physics 2019, 52 (22), 224002.
  - 18. Hong, J.; Steven, P.; Anthony, B., Murphy., Plasma catalysis as an alternative route for ammonia
- production: status, mechanisms, and prospects for progress. ACS Sustainable Chemistry & Engineering 2018, 6 (1), 15-31.
- 47 19. Hong, J.; Prawer, S.; Murphy, A. B., Production of ammonia by heterogeneous catalysis in a packed-bed
- dielectric-barrier discharge: influence of argon addition and voltage. *IEEE Transactions on Plasma Science* **2014**,
- 49 42 (10), 2338-2339.

- Patil, B. S.; van Kaathoven, A. S.; Peeters, F.; Cherkasov, N.; Wang, Q.; Lang, J.; Hessel, V., 1 20.
- 2 Deciphering the synergy between plasma and catalyst support for ammonia synthesis in a packed DBD reactor.
- 3 Journal of Physics D: Applied Physics 2020.
- 4 Peng, P.; Li, Y.; Cheng, Y.; Deng, S.; Chen, P.; Ruan, R., Atmospheric pressure ammonia synthesis 5 using non-thermal plasma assisted catalysis. *Plasma Chemistry and Plasma Processing* **2016**, *36* (5), 1201-1210.
- 6 Akay, G., & Zhang, K., Process intensification in ammonia synthesis using novel coassembled supported 22. 7 microporous catalysts promoted by nonthermal plasma. Industrial & Engineering Chemistry Research 2017, 56
  - (2), 457-468.

11

19

20

23

26

42

- 9 Shah, J.; Wu, T.; Lucero, J.; Carreon, M. A.; Carreon, M. L., Nonthermal plasma synthesis of ammonia 23. 10 over Ni-MOF-74. ACS Sustainable Chemistry & Engineering 2018, 7(1), 377-383.
  - Shah, J. R.; Gorky, F.; Lucero, J.; Carreon, M. A.; Carreon, M. L., Ammonia synthesis via atmospheric
- plasma-catalysis: Zeolite 5A a case of study. *Industrial & Engineering Chemistry Research* **2020**. 12 13 Gorky, F.; Carreon, M. A.; Carreon, M. L., Experimental strategies to increase ammonia yield in plasma
- 14 catalysis over LTA and BEA zeolites. *IOP SciNotes* **2020**, *1* (2), 024801. 15 26. Carreon, M. A., Porous crystals as membranes. *Science* **2020**, *367* (6478), 624-625.
- Feng, X.; Zong, Z.; Elsaidi, S. K.; Jasinski, J. B.; Krishna, R.; Thallapally, P. K.; Carreon, M. A., Kr/Xe 16 27. separation over a chabazite zeolite membrane. Journal of the American Chemical Society 2016, 138 (31), 9791-
- 17 18 9794.
  - Feng, X.; Carreon, M.A. Kinetics of Transformation on ZIF-67 Crystals. Journal of Crystal Growth 2015, 28. *418*, 158-162.
- 21 29. Gorky, F.; Best, A.; Jasinski, J.; Allen, B. J.; Alba-Rubio, A. C.; Carreon, M. L., Plasma catalytic 22 ammonia synthesis on Ni nanoparticles: the size effect. Journal of Catalysis 2020.
  - Park, K. S.; Ni, Z.; Côté, A. P.; Choi, J. Y.; Huang, R.; Uribe-Romo, F. J.; Chae, H. K.; O'Keeffe,
- 24 M.; Yaghi, O. M., Exceptional chemical and thermal stability of zeolitic imidazolate frameworks. *Proceedings of* 25 the National Academy of Sciences **2006**, 103 (27), 10186-10191.
  - Iwamoto, M.; Akiyama, M.; Aihara, K.; Deguchi, T., Ammonia synthesis on wool-like Au, Pt, Pd, Ag,
- 27 or Cu electrode catalysts in nonthermal atmospheric-pressure plasma of N2 and H2. ACS Catalysis 2017, 7 (10), 28 6924-6929.
- 29 Shah, J.; Wang, W.; Bogaerts, A.; Carreon, M. L., Ammonia synthesis by radio frequency plasma 32. 30
  - catalysis: revealing the underlying mechanisms. ACS Applied Energy Materials 2018, 1 (9), 4824-4839.
- 31 Mehta, P.; Barboun, P. M.; Engelmann, Y.; Go, D. B.; Bogaerts, A.; Schneider, W. F.; Hicks, J. C., 32
  - Plasma-catalytic ammonia synthesis beyond the equilibrium limit. ACS Catalysis 2020, 10 (12), 6726-6734.
- 33 Yuan, S.; Feng, L.; Wang, K.; Pang, J.; Bosch, M.; Lollar, C.; Sun, Y.; Qin, J.; Yang, X.; Zhang, P.,
- 34 Stable metal-organic frameworks: design, synthesis, and applications. Advanced Materials 2018, 30 (37),
- 35 1704303.
- 36 35. Li, S.; Van Raak, T.; Gallucci, F., Investigating the operation parameters for ammonia synthesis in
- dielectric barrier discharge reactors. Journal of Physics D: Applied Physics 2019, 53 (1), 014008. 37
- Butterworth, T.; Elder, R.; Allen, R., Effects of particle size on CO2 reduction and discharge 38 36.
- 39 characteristics in a packed bed plasma reactor. Chemical Engineering Journal 2016, 293, 55-67.
- 40 Wang, Y.; Craven, M.; Yu, X.; Ding, J.; Bryant, P.; Huang, J.; Tu, X., Plasma-enhanced catalytic 41
  - synthesis of ammonia over a Ni/Al2O3 catalyst at near-room temperature: Insights into the importance of the catalyst surface on the reaction mechanism. ACS Catalysis 2019, 9 (12), 10780-10793.

# 1 Table of Contents

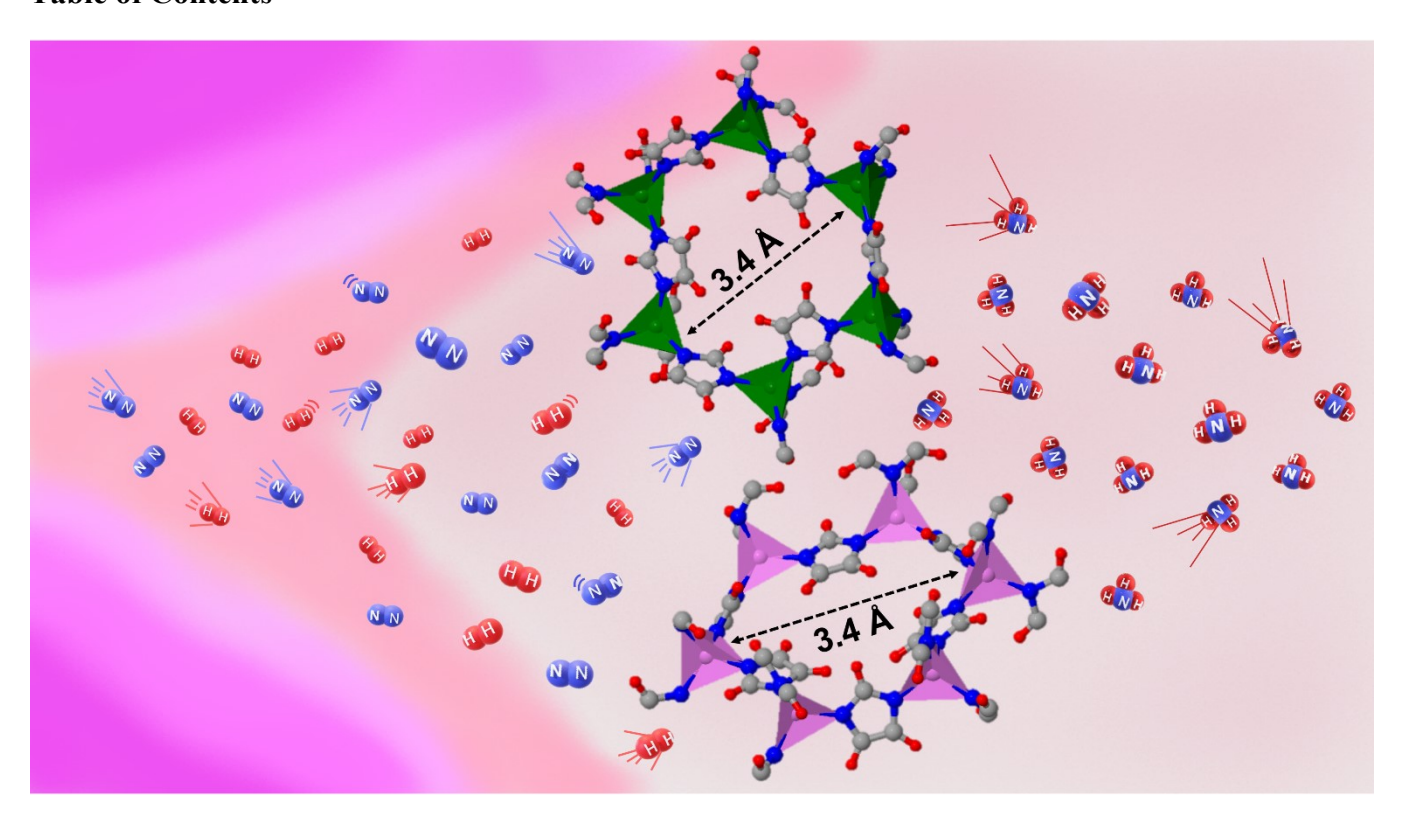


**Table of Contents (TOC) Graphic.** Plasma catalytic ammonia synthesis over ZIF-8 and ZIF-67.